

Framework for evaluating the performance limits of membraneless electrolyzers

Supporting Information

Xueqi Pang,¹ Jonathan T. Davis,¹ Albert D. Harvey III,² Daniel V. Esposito^{1,^}

¹Columbia University in the City of New York

Department of Chemical Engineering

Columbia Electrochemical Energy Center

Lenfest Center for Sustainable Energy

500 W. 120th St., New York, NY 10027, USA

²Shell International Exploration & Production, Inc.

3333 Highway 6 South, Houston, TX 77082, USA

[^]corresponding author: de2300@columbia.edu

Table of Contents

S1. Schematic of the assembled flow cell.....	2
S2. Schematic of the experimental setup.....	3
S3. % H₂ collected in gas-phase as a function of <i>Re</i> and current density	4
S4. Relationships between % H₂ crossover and H₂ % in the anode and cathode effluents.....	5
S5. Current density-voltage curves for electrolyzers with different channel widths	7
S6. EIS measurements for electrolyzers with different channel widths.....	8
S7. Average H₂ bubble diameter as a function of <i>Re</i>	9
S8. H₂ bubble size distribution.....	10
S9. Correlation between 2D bubble coverage and 3D void fraction.....	11
S10. Contour maps.....	13
S11. H₂ crossover and normalized H₂ bubble plume width at different <i>Re</i> for electrolysis at a constant current density of 200 mA cm⁻²	14
S12. H₂ crossover and normalized H₂ bubble plume width at different <i>Re</i> for electrolysis at a constant current density of 400 mA cm⁻²	15
S13. The ratio of pumping power to the generated power as a function of <i>Re</i>.....	16
S14. H₂ crossover as a function of normalized H₂ bubble plume width in the laminar flow regime .	17
S15. H₂ crossover as a function of normalized H₂ bubble plume width for all operating conditions	18
S16. H₂ crossover as a function of normalized H₂ bubble plume width at different current densities for electrolysis at a constant <i>Re</i> of 796	19
S17. H₂ crossover as a function of normalized H₂ bubble plume width at different current densities for electrolysis at a constant <i>Re</i> of 131	20
S18. H₂ plume width as a function of <i>Da</i>^{0.47} in the laminar flow regime	21
S19. Solution resistance as a function of channel width for different electrode lengths.....	22
S20. Bubble-induced ohmic drop.....	23
S21. Current density-voltage curves from experimental measurement and 1D model	24
S22. “Big bubble” departure event.....	25
Video	26
References.....	27

S1. Schematic of the assembled flow cell

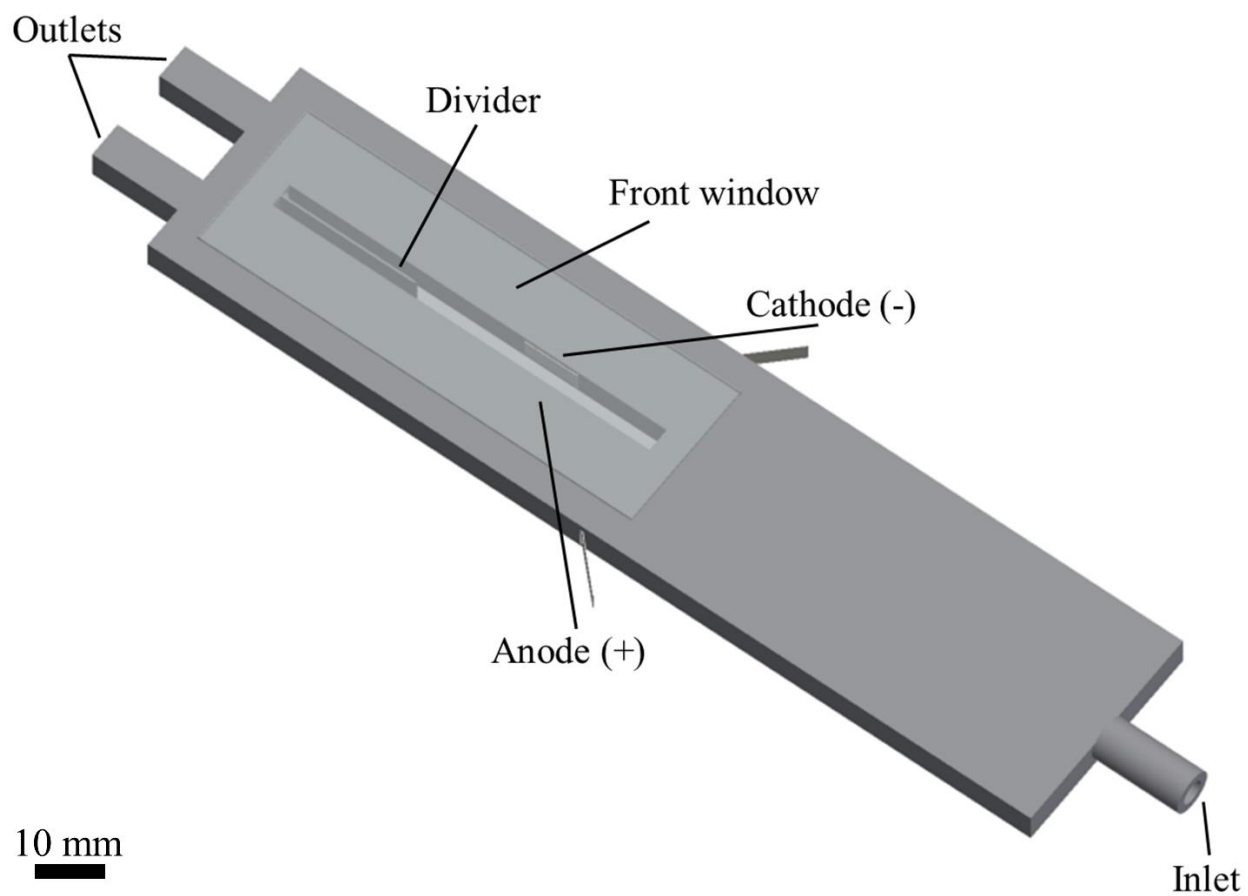


Figure S1: Computer aided design rendering of the assembled cell. The channel width for the cell shown here is 4 mm.

S2. Schematic of the experimental setup

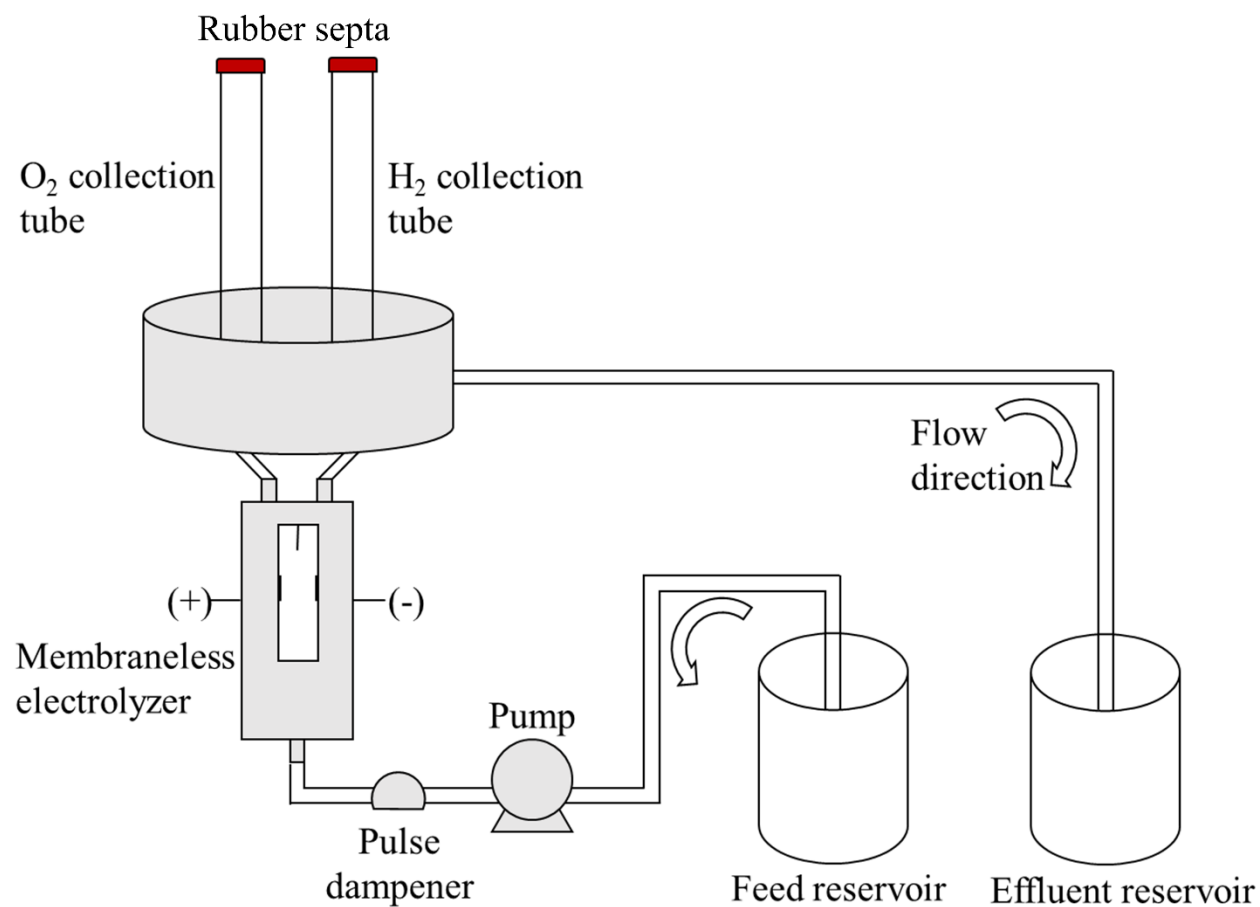


Figure S2: Flow diagram of the experimental set-up.

S3. % H₂ collected in gas-phase as a function of *Re* and current density

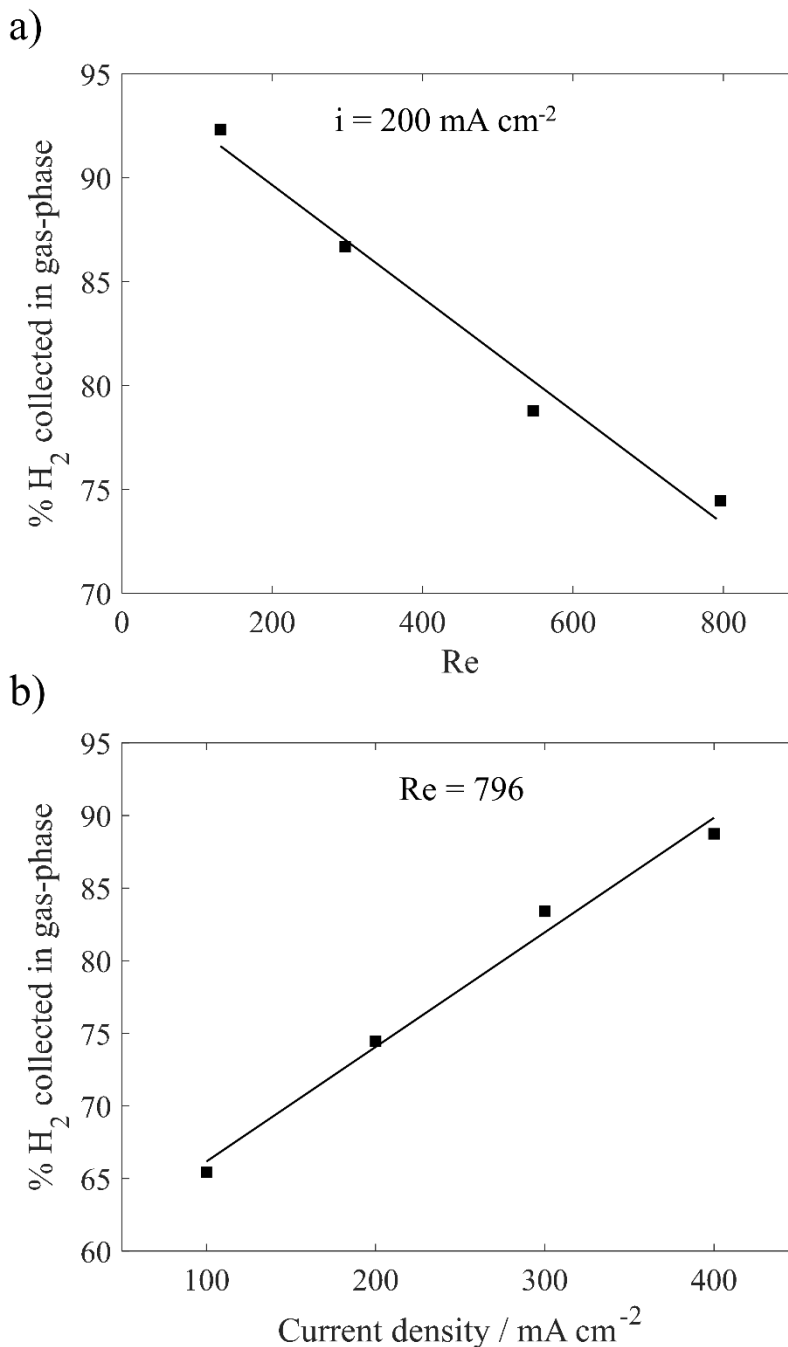


Figure S3: a) % H₂ collected in gas-phase as a function of *Re* for constant current density of 200 mA cm⁻². b) % H₂ collected in gas-phase as a function of current density at constant *Re* of 796. Volume of H₂ collected in gas-phase was determined by measuring the volume of gas products collected in the two gas collection tubes and quantifying H₂ % in each gas collection tube by GC. The maximum possible H₂ gas volume was calculated by Faraday's law, assuming a 100% H₂ Faradaic efficiency. % H₂ collected in gas-phase was determined using the volume of collected H₂ gas divided by the maximum possible H₂ gas volume.

S4. Relationships between % H₂ crossover and H₂ % in the anode and cathode effluents

If one assumes all products generated are in the gas phase. Based on the stoichiometry of water splitting, 2 moles of H₂ gas are produced at the cathode for every 1 mole of O₂ gas produced at the anode. The flammable / explosive hazard will likely to occur in the O₂ collection chamber when the crossover of gas products is too high. H₂ crossover was calculated by using the amount of H₂ that crossed over to the anode effluent stream dividing by the total amount of produced H₂. Therefore, from a safety standpoint, % H₂ crossover is plotted as a function of H₂ % in the anode effluent for different ratios of H₂ crossover to O₂ crossover. It is essential to maintain the H₂ % in the anode effluent to be lower than 4%, which is the lower flammability limit (LFL) for H₂ in O₂.¹ % H₂ crossover is also plotted as a function of H₂ purity.

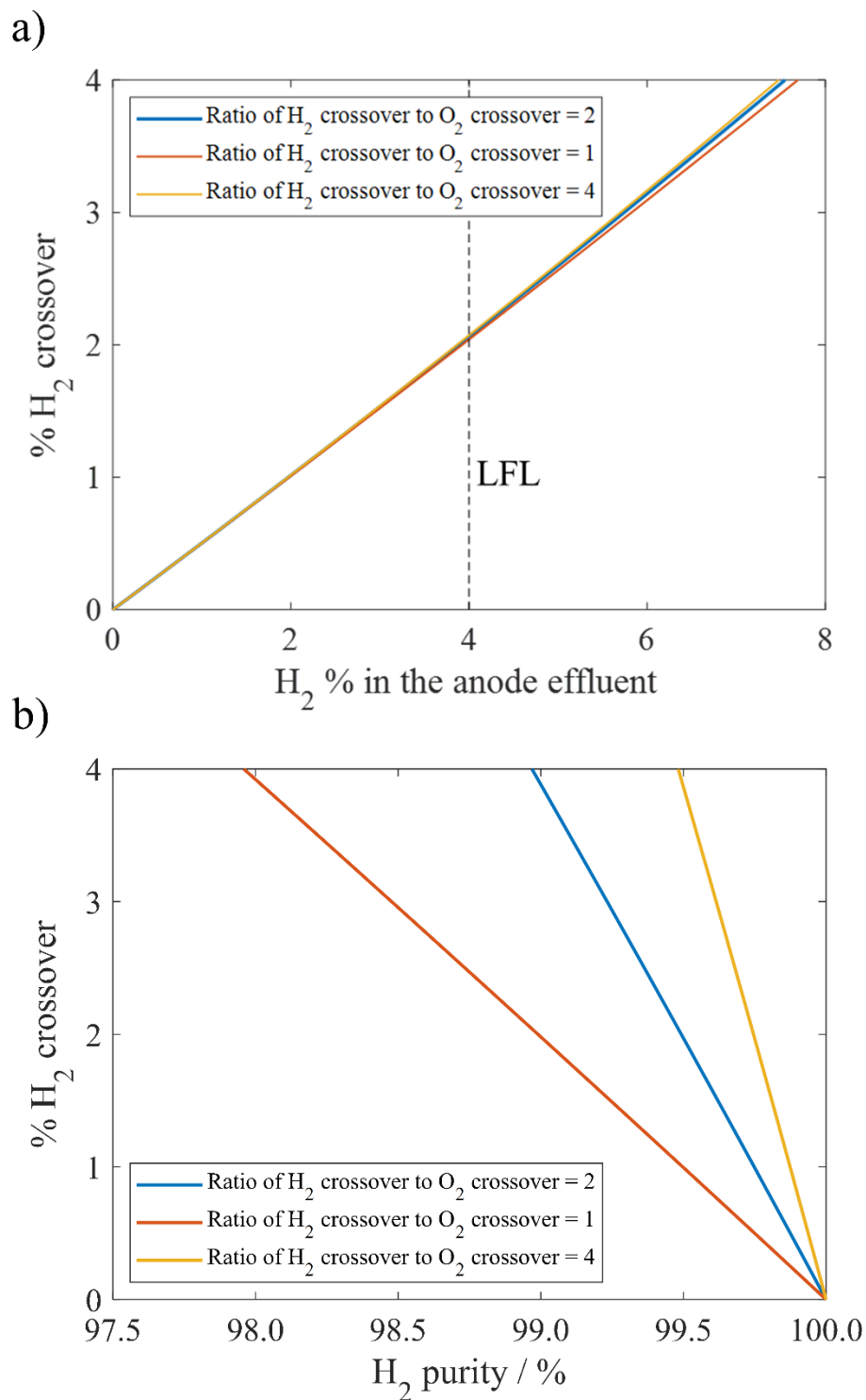


Figure S4: a) Relationships between % H₂ crossover and atomic % H₂ in the anode effluent for different ratios of H₂ crossover to O₂ crossover. LFL for H₂ in O₂ is 4%.¹ b) % H₂ crossover as a function of H₂ purity for different ratios of H₂ crossover to O₂ crossover.

S5. Current density-voltage curves for electrolyzers with different channel widths

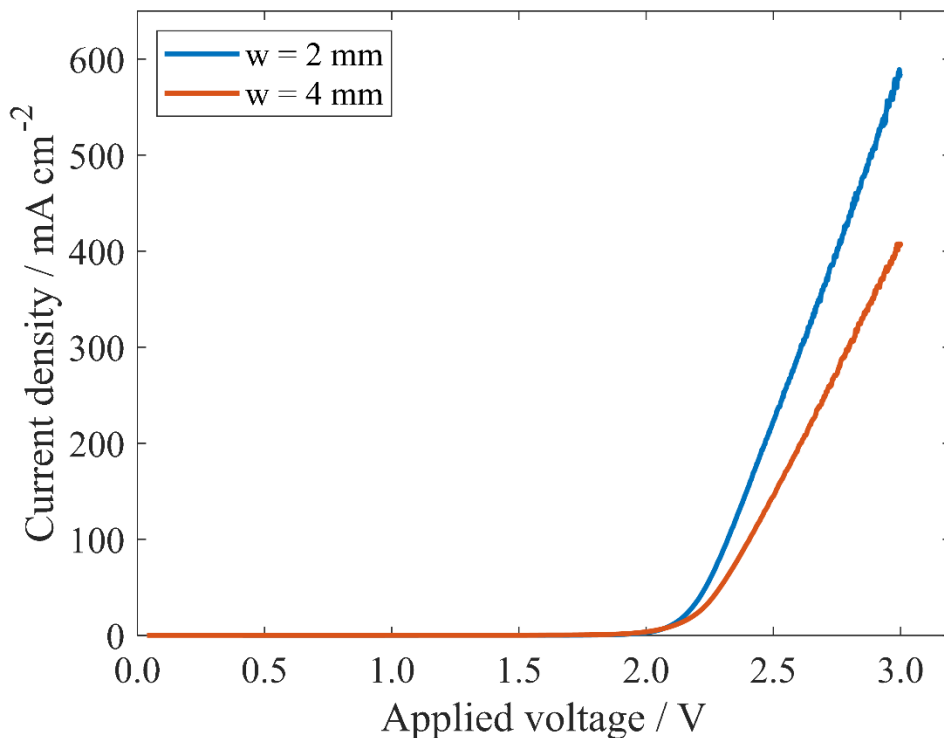


Figure S5: 2-electrode current density-voltage curves of water electrolysis with 0.5 M H₂SO₄ containing surfactant at a scan rate of 10 mV s⁻¹ for electrolyzers with 2 mm and 4 mm channel widths at the same *Re* of 547. Platinized Ti foil electrodes were used as both cathode and anode. A significant increase in the slope of iV curve of the 2 mm cell compared to the 4 mm cell results from the smaller solution resistance associated with the smaller electrode gap.

S6. EIS measurements for electrolyzers with different channel widths

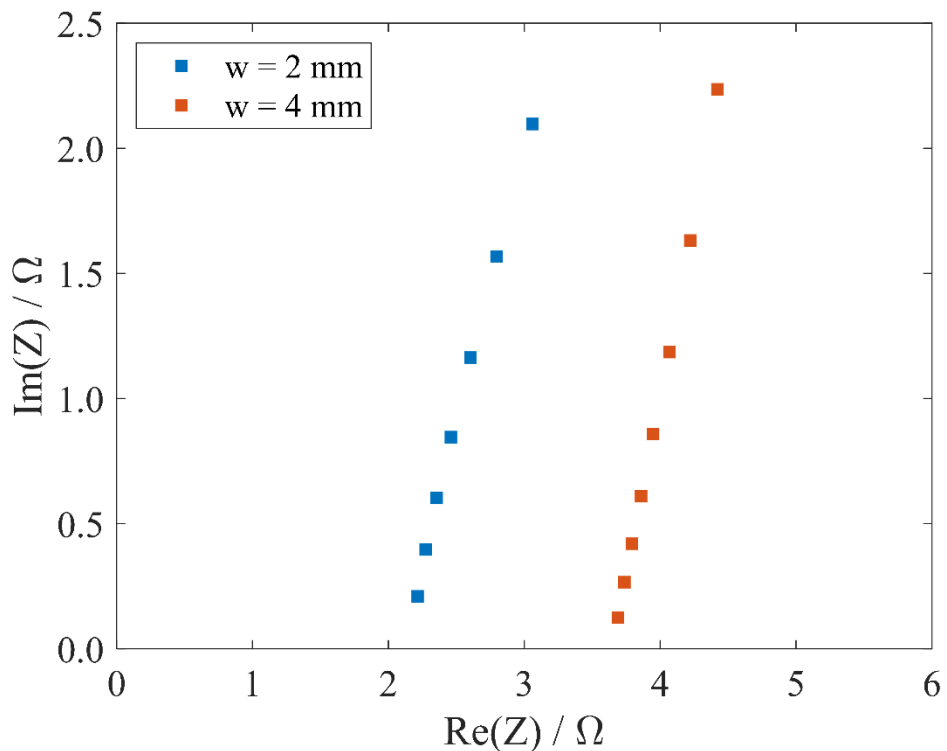


Figure S6: EIS measurements for water electrolysis with 0.5 M H_2SO_4 containing surfactant for electrolyzers with 2 mm and 4 mm channel widths. EIS measurements were conducted at a constant applied cell voltage of 0.2 V vs. open circuit potential using an AC amplitude of 10 mV with a frequency range between 100 mHz and 200 kHz. 2 mm cell has a lower ohmic resistance due to smaller electrode gap.

S7. Average H₂ bubble diameter as a function of Re

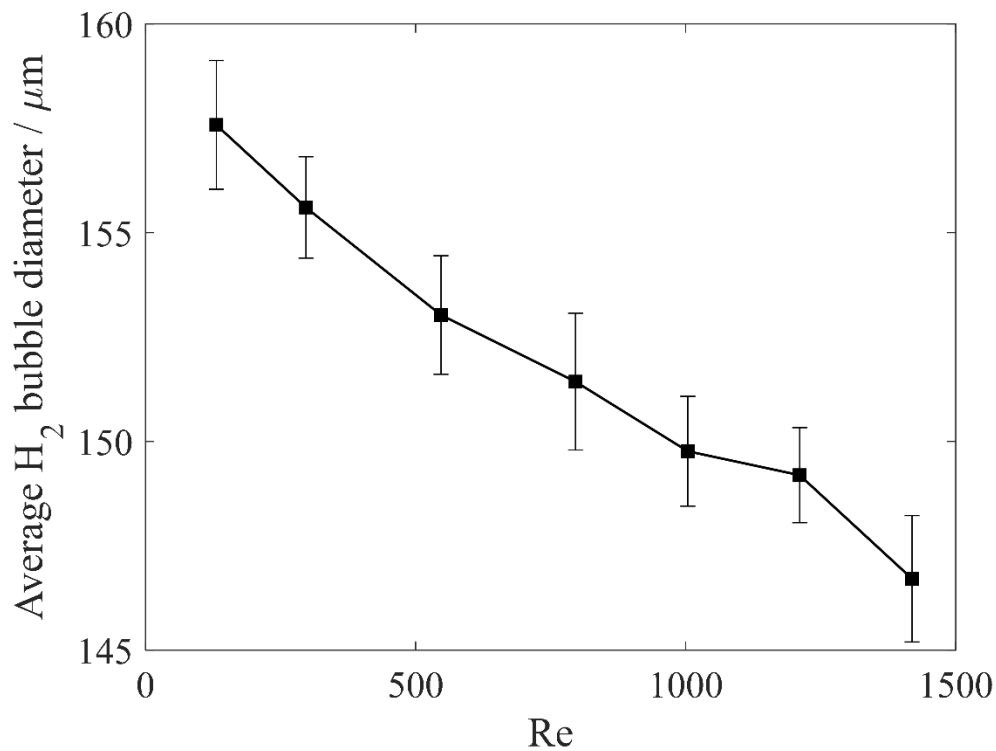


Figure S7: Average H₂ bubble size as a function of Re for water electrolysis in surfactant-containing 0.5 M H₂SO₄ at 200 mA cm⁻² in a $w = 4$ mm cell. Error bars were determined by calculating the 95% confidence interval based on averaging the average bubble size over 100 frames.

S8. H₂ bubble size distribution

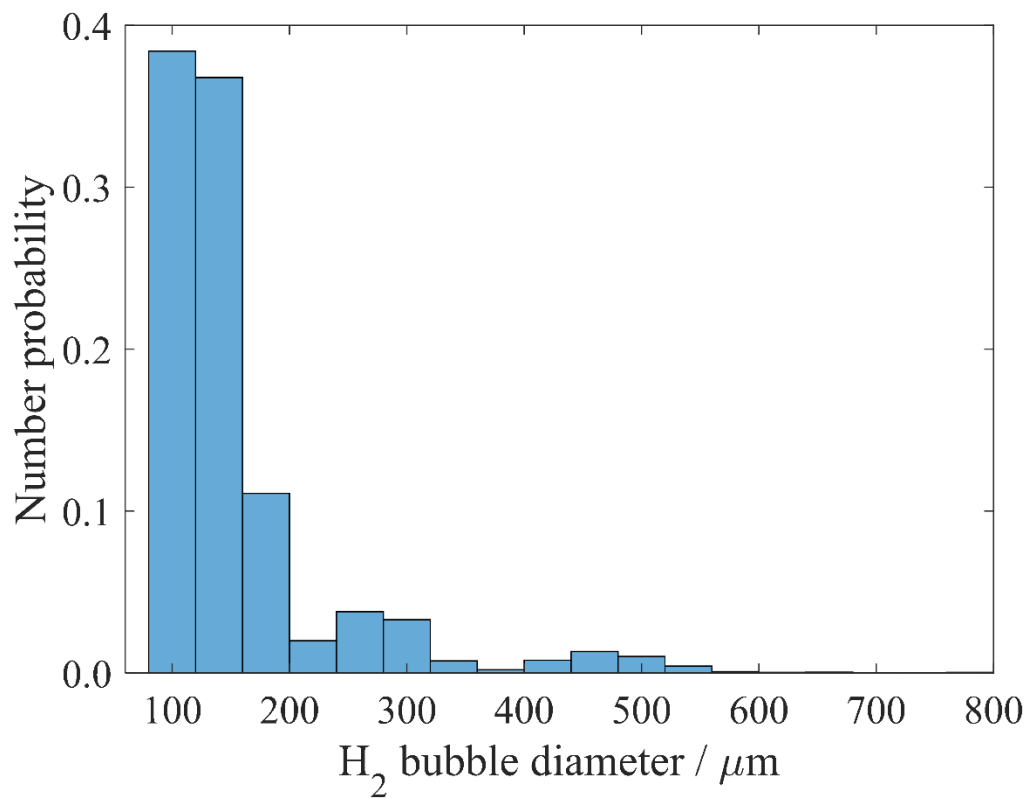


Figure S8: H₂ bubble size distribution determined from HSV for water electrolysis in surfactant-containing 0.5 M H₂SO₄ at $Re = 796$ and 200 mA cm^{-2} in a 4 mm cell.

S9. Correlation between 2D bubble coverage and 3D void fraction

As shown in Figure 3d in the main article, maps of average 2D bubble coverage were derived from 300 still frame images taken from HSVs. It's necessary to convert the 2D coverage into 3D bubble void fraction because H_2 crossover rate depends on the volume of H_2 bubbles that cross over to the anode effluent stream. In order to accurately determine the relationship between 2D coverage and 3D void fraction, MATLAB was used to generate 3D images of bubbles within a 5 mm deep x 2 mm wide by 9 mm long control volume which has the same depth as the channel of the PPME used in this study. Bubbles with size distribution corresponding to those observed in experiment at 200 mA cm^{-2} and $Re = 796$ (Figure S7) were randomly positioned within this control volume. One example is shown in Figure S8a with a void fraction of 0.032 and bubble coverage of 0.62. The color of each bubble indicates the z location. The bubble void fraction was calculated based on the number and known radii of all generated bubbles. Bubble coverage was calculated based on white and non-white pixels of the 2D projection of bubbles in this 3D image, which can be seen in the third image of Figure S8b. Moreover, 2D projections with other bubble coverages were also presented in Figure S8b. Since a higher bubble density gave rise to a higher bubble coverage, finding the aforementioned correlation is crucial. Hence, the true relationship was generated based on the 2D coverage and real void fraction, as shown in Figure S8c (blue curve). If the bubble overlap was neglected, the 2D projected area of bubbles could be converted into volume by multiplying the area of bubbles by $(4/3)$ times the average radius of the bubbles, shown in Figure S8c (red curve). Consequently, neglecting bubble overlap will underestimate bubble coverage for coverage higher than 0.2. With increasing bubble coverage, this underestimation will be more significant. Therefore, it's necessary to apply this relationship to accurately convert the local average 2D coverage of bubbles measured in HSV still frames to 3D void fraction on a pixel by pixel basis in order to generate accurate bubble void fraction maps such as those provided in Figure 4 of the main article.

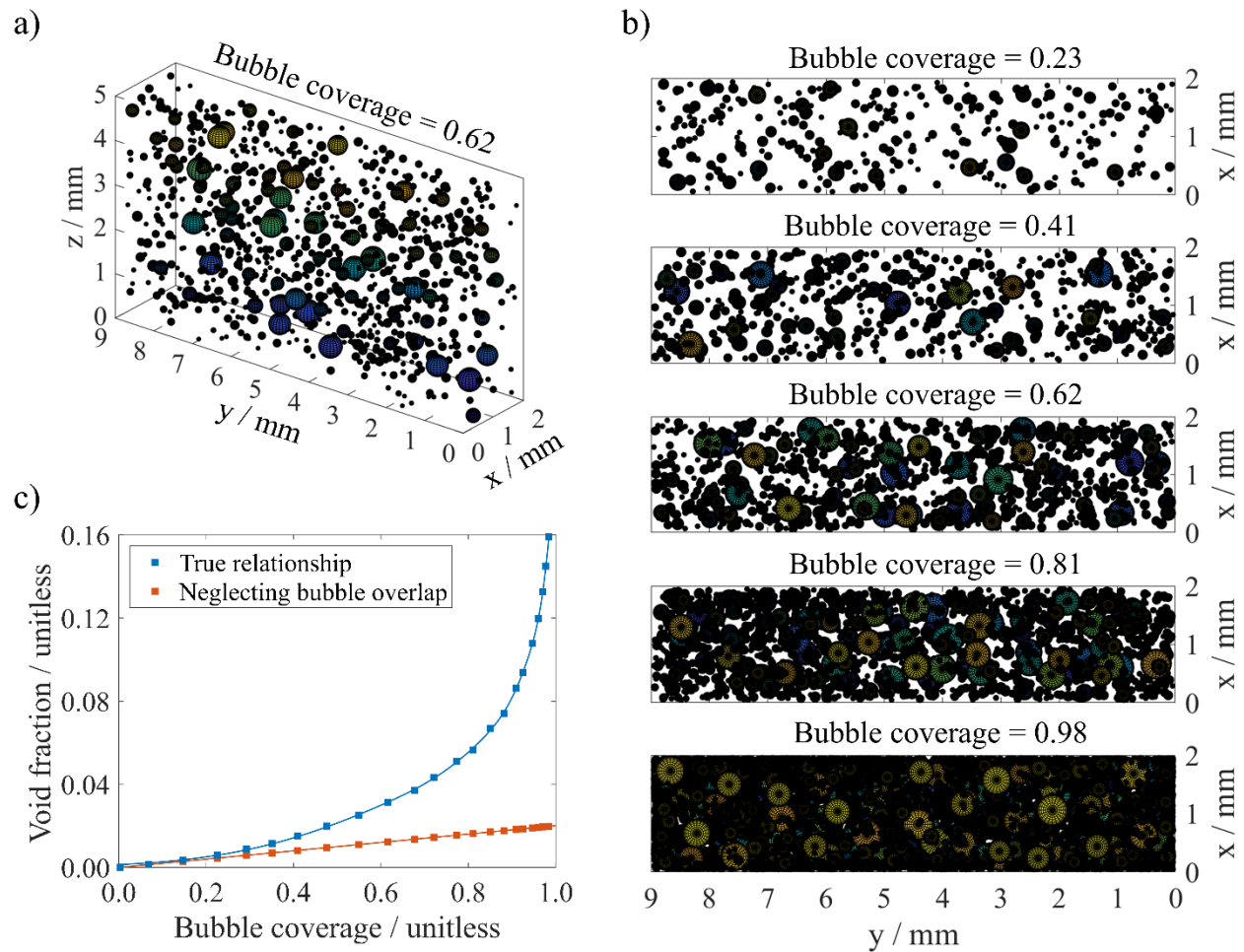


Figure S9: a) Computer-generated 3D image of bubbles of different size randomly positioned within a 5 mm deep x 2 mm wide by 9 mm long control volume and characterized by a total void fraction of 0.032. The bubble size distribution used to generate this image was derived from bubble detection algorithm for a HSV corresponding to an electrolysis experiment at 200 mA cm^{-2} and $Re = 796$. b) 2D projections of bubbles located in 3D spaces for different bubble coverages. c) Computer-generated true relationship between the 2D bubble coverage and 3D bubble void fraction and the linear correlation neglecting bubble overlap for a cell depth of 5 mm.

S10. Contour maps

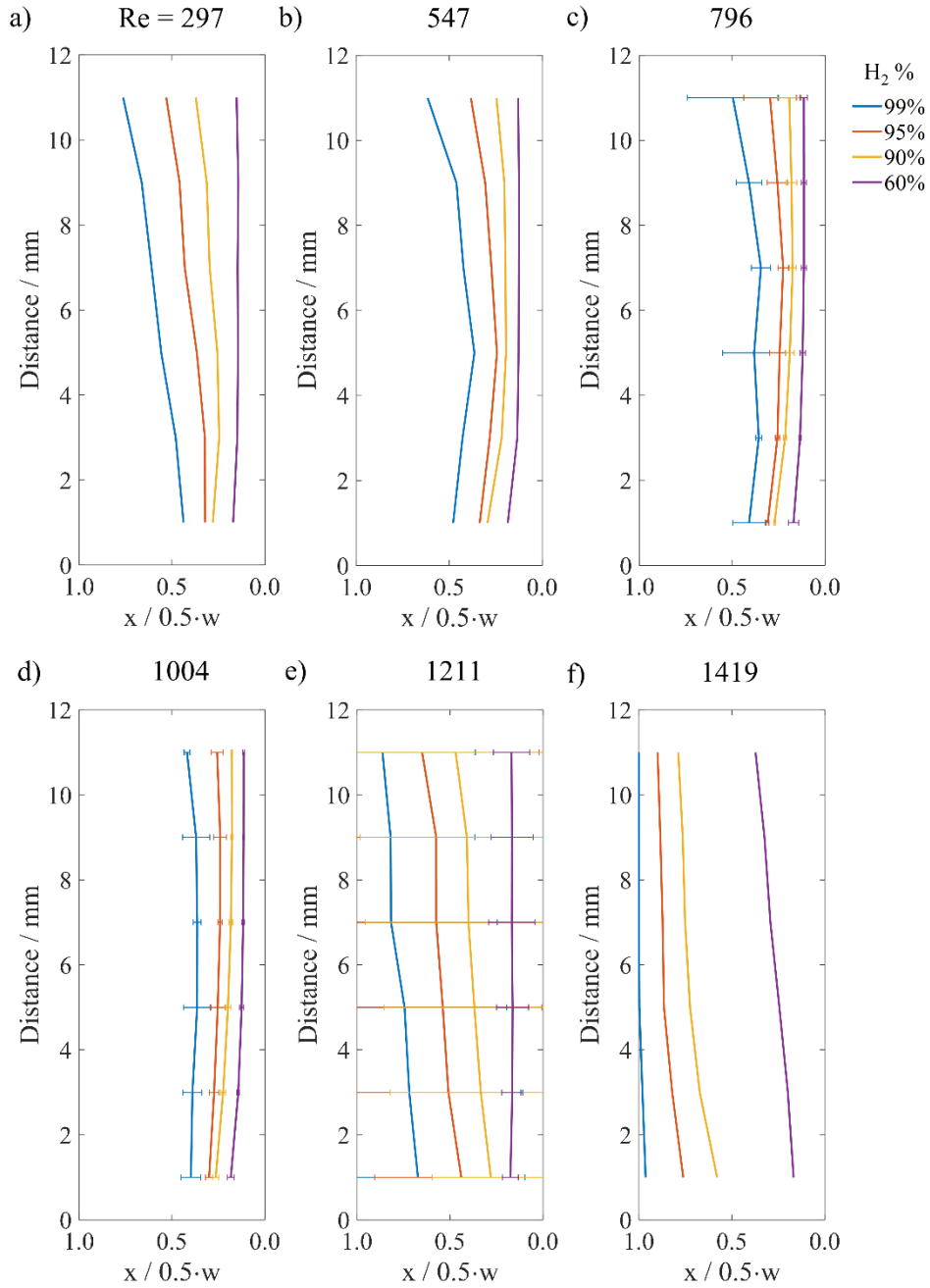


Figure S10: Contour lines from the void fraction images in Figure 4b-g that correspond to the locations where 99%, 95%, 90% and 60% of H₂ within the plume is located to the right of the line.

S11. H₂ crossover and normalized H₂ bubble plume width at different *Re* for electrolysis at a constant current density of 200 mA cm⁻²

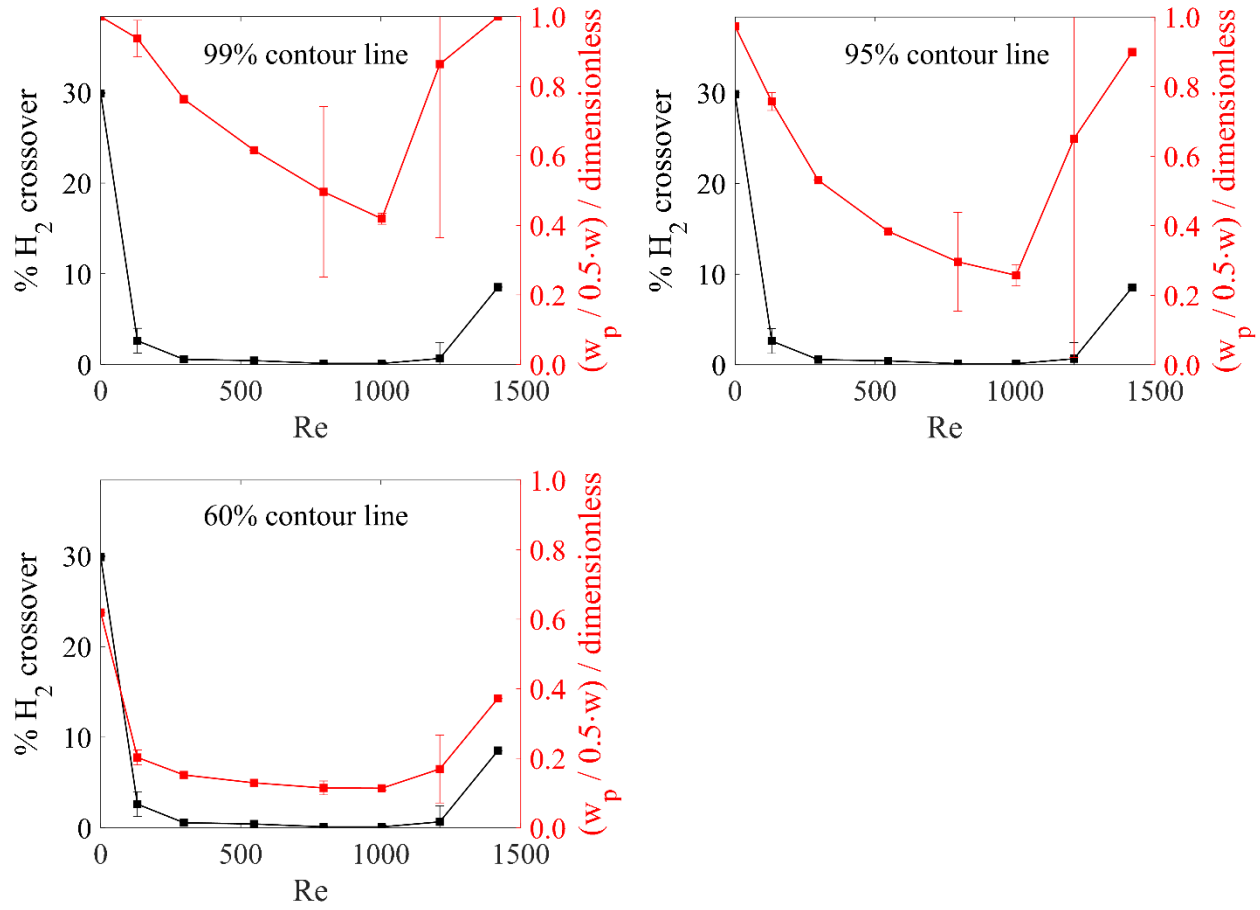


Figure S11: H₂ crossover and normalized H₂ bubble plume width at different *Re* for electrolysis at a constant current density of 200 mA cm⁻² when using different percentage contour line values (*X* = 99%, 95%, 60%) as the normalized bubble plume widths. Channel width is 4 mm.

S12. H₂ crossover and normalized H₂ bubble plume width at different *Re* for electrolysis at a constant current density of 400 mA cm⁻²

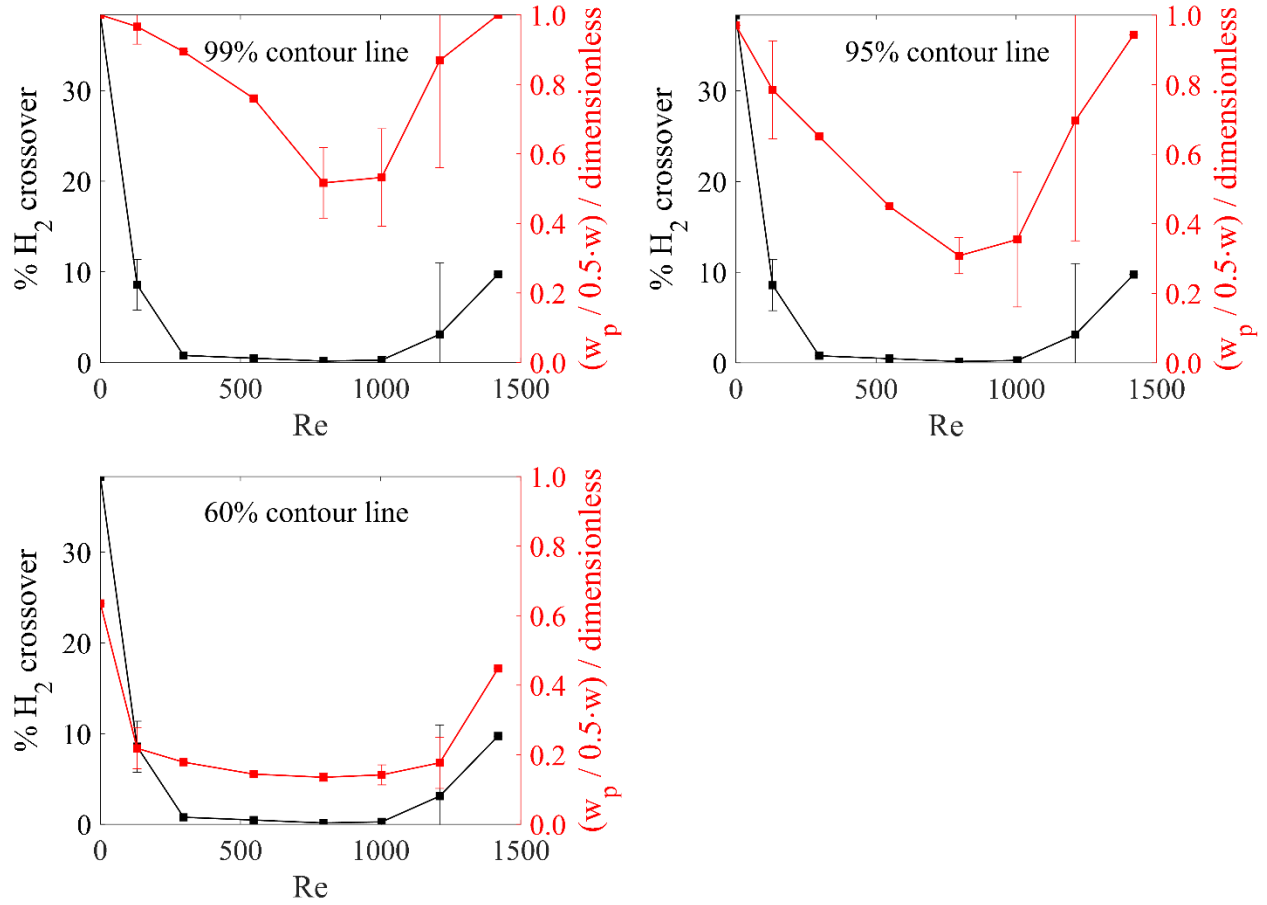


Figure S12: H₂ crossover and normalized H₂ bubble plume width at different *Re* for electrolysis at a constant current density of 400 mA cm⁻² when using different percentage contour line values (*X* = 99%, 95%, 60%) as the normalized bubble plume widths. Channel width is 4 mm.

S13. The ratio of pumping power to the generated power as a function of Re

In laminar flow, the pressure drop (ΔP) inside the fluidic channel can be calculated using Bernoulli's equation neglecting friction²:

$$P + \frac{1}{2}\rho V^2 + \rho g z = constant$$

where P is the pressure, ρ is density of the fluid, V is the fluid flow velocity, g is the acceleration due to gravity, and z is the elevation.

Assume ρ and V are constants,

$$\Delta P = -\rho g \Delta z$$

$\rho = 1.03 \text{ g mL}^{-1}$, density of 0.5 M H_2SO_4

Since the electrolyzer is oriented vertically, for a 145 mm long fluidic channel length, $\Delta P = 1465.1$ Pa. The pumping power is the product of ΔP and volumetric flow rate, where the pump efficiency is assumed to be 75%. The generated H_2 power is the product of 1.23 V and current.

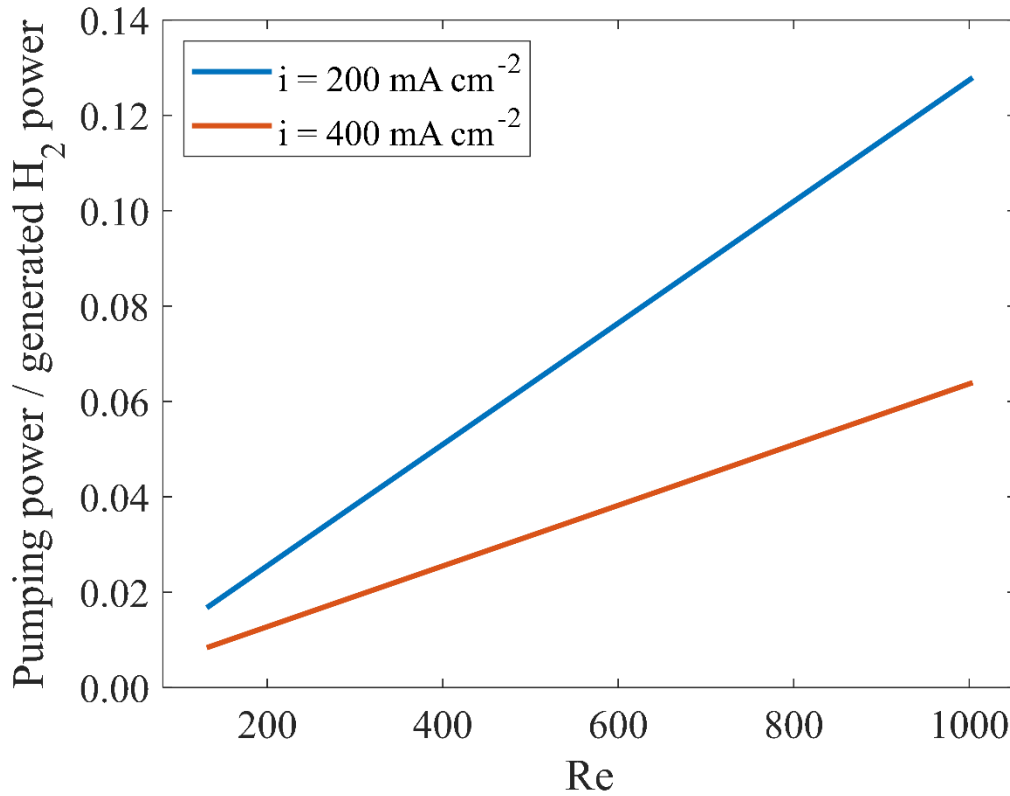


Figure S13: The ratio of required pumping power to the generated power as a function of Re at 200 and 400 mA cm^{-2} . The pump efficiency is assumed to be 75%.

S14. H₂ crossover as a function of normalized H₂ bubble plume width in the laminar flow regime

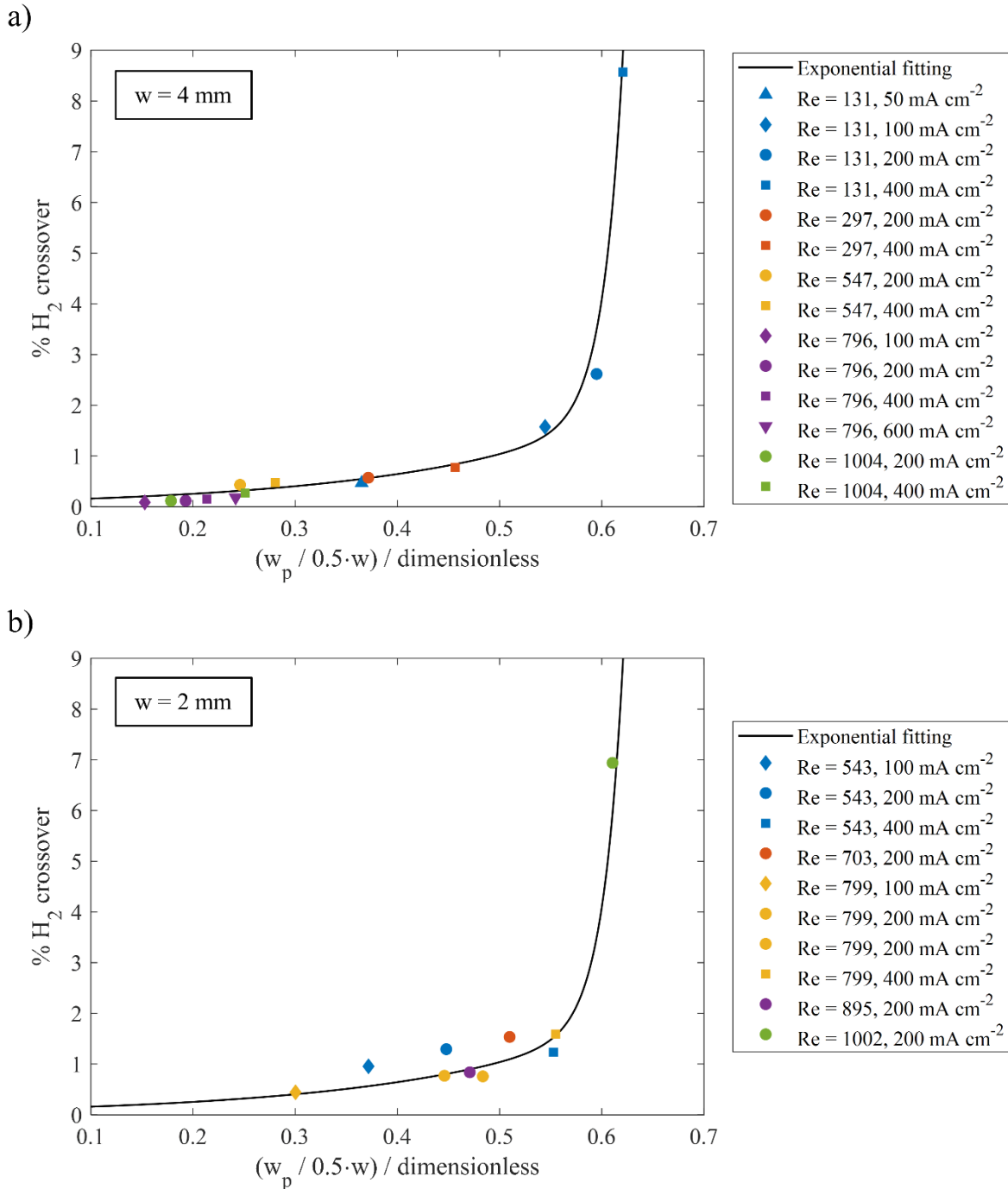


Figure S14: a) H₂ crossover as a function of normalized H₂ bubble plume width for $w = 4$ mm at different current densities in the laminar flow regime with an exponential fitting. b) H₂ crossover as a function of normalized H₂ bubble plume width for $w = 2$ mm at different current densities in the laminar flow regime with an exponential fitting. 90% contour line values are used as the normalized bubble plume widths.

S15. H₂ crossover as a function of normalized H₂ bubble plume width for all operating conditions

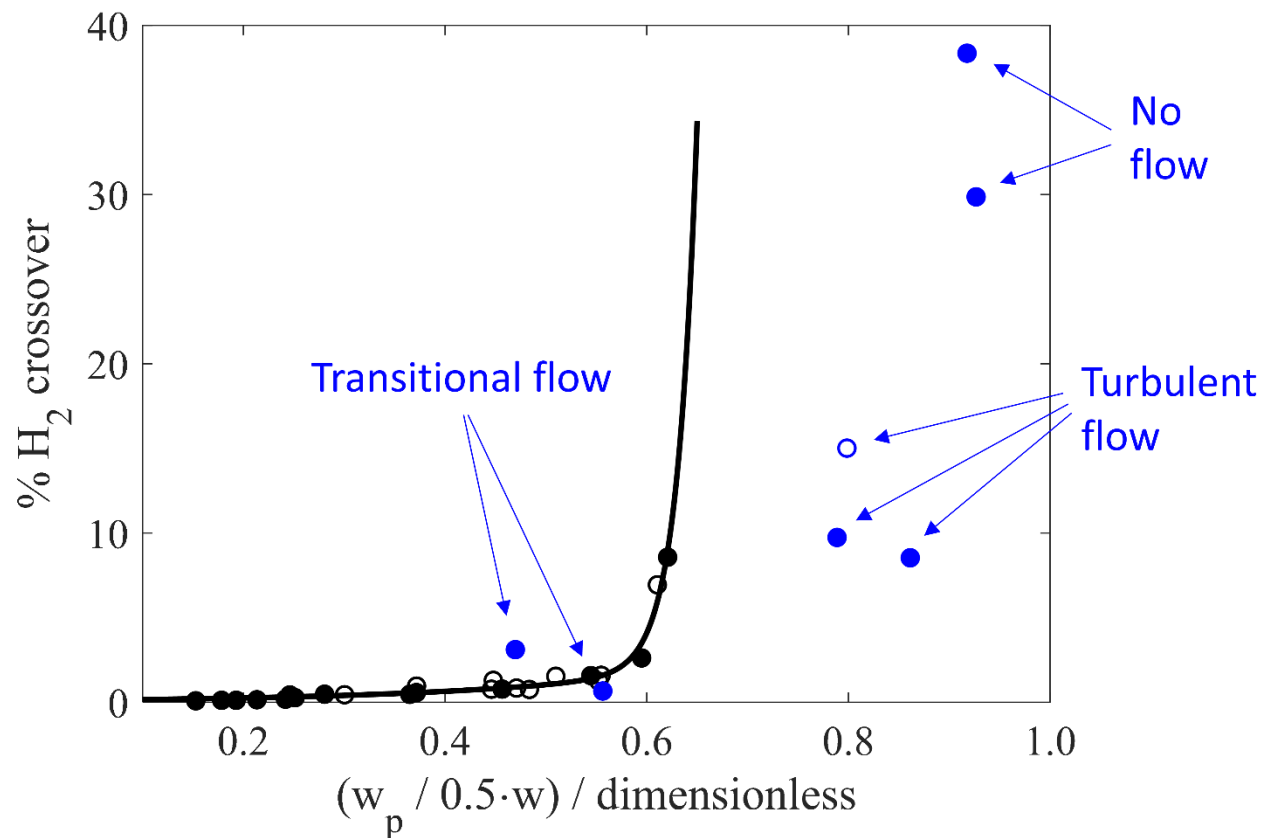


Figure S15: a) H₂ crossover as a function of normalized H₂ bubble plume width for 2 different channel widths and all operating conditions including the transitional flow, turbulent flow and no flow conditions. Data points were obtained for measurements recorded with cells based on $w = 4$ mm (solid circles) and $w = 2$ mm (open circles). The black line is an exponential fitting for all operating conditions in the laminar flow regime. 90% contour line values are used as the normalized bubble plume widths.

S16. H₂ crossover as a function of normalized H₂ bubble plume width at different current densities for electrolysis at a constant *Re* of 796

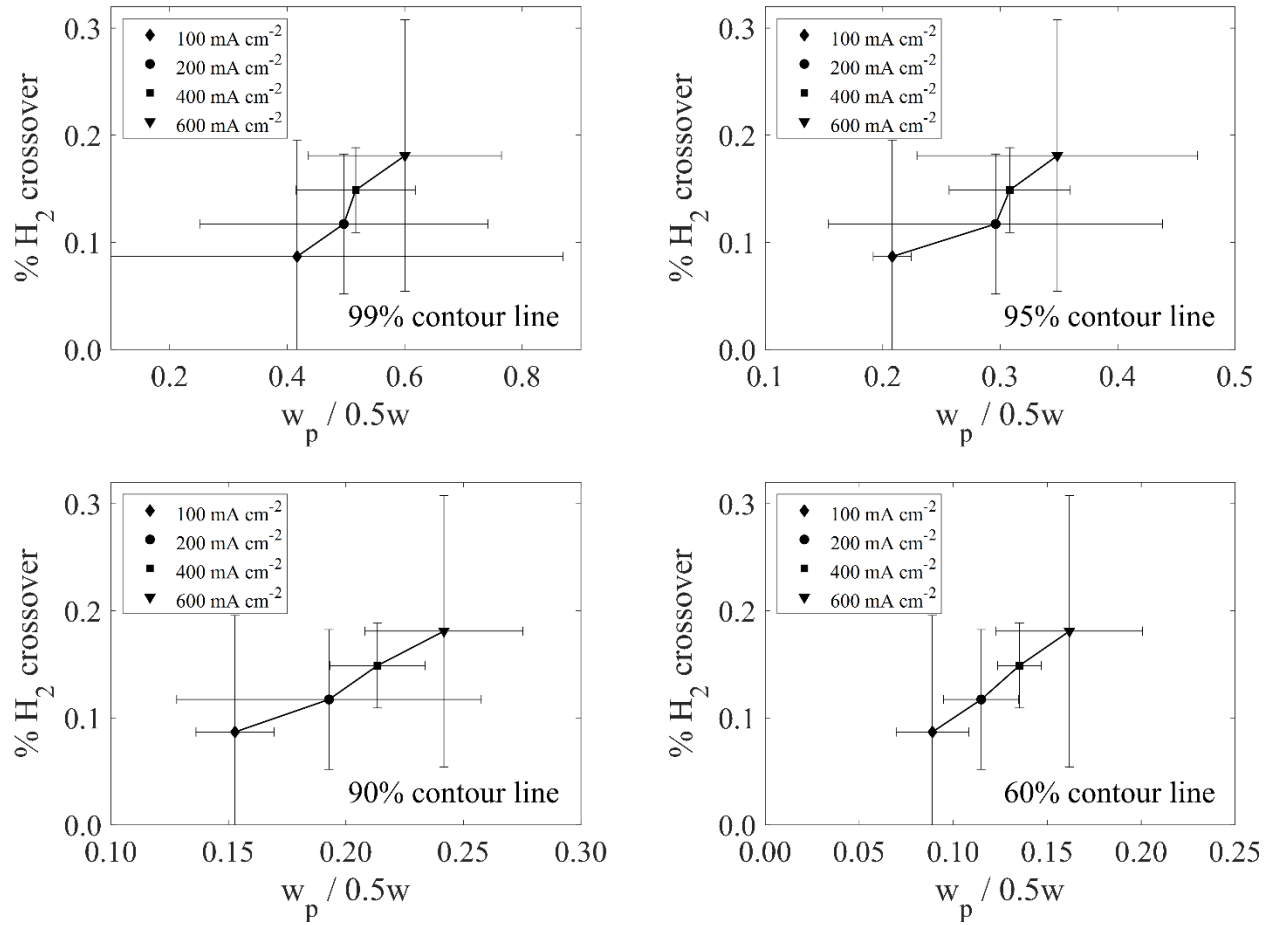


Figure S16: H₂ crossover as a function of normalized H₂ bubble plume width at different current densities for electrolysis at a constant *Re* of 796 when using different percentage contour line values (*X* = 99%, 95%, 90%, 60%) as the normalized bubble plume widths. Channel width is 4 mm.

S17. H₂ crossover as a function of normalized H₂ bubble plume width at different current densities for electrolysis at a constant *Re* of 131

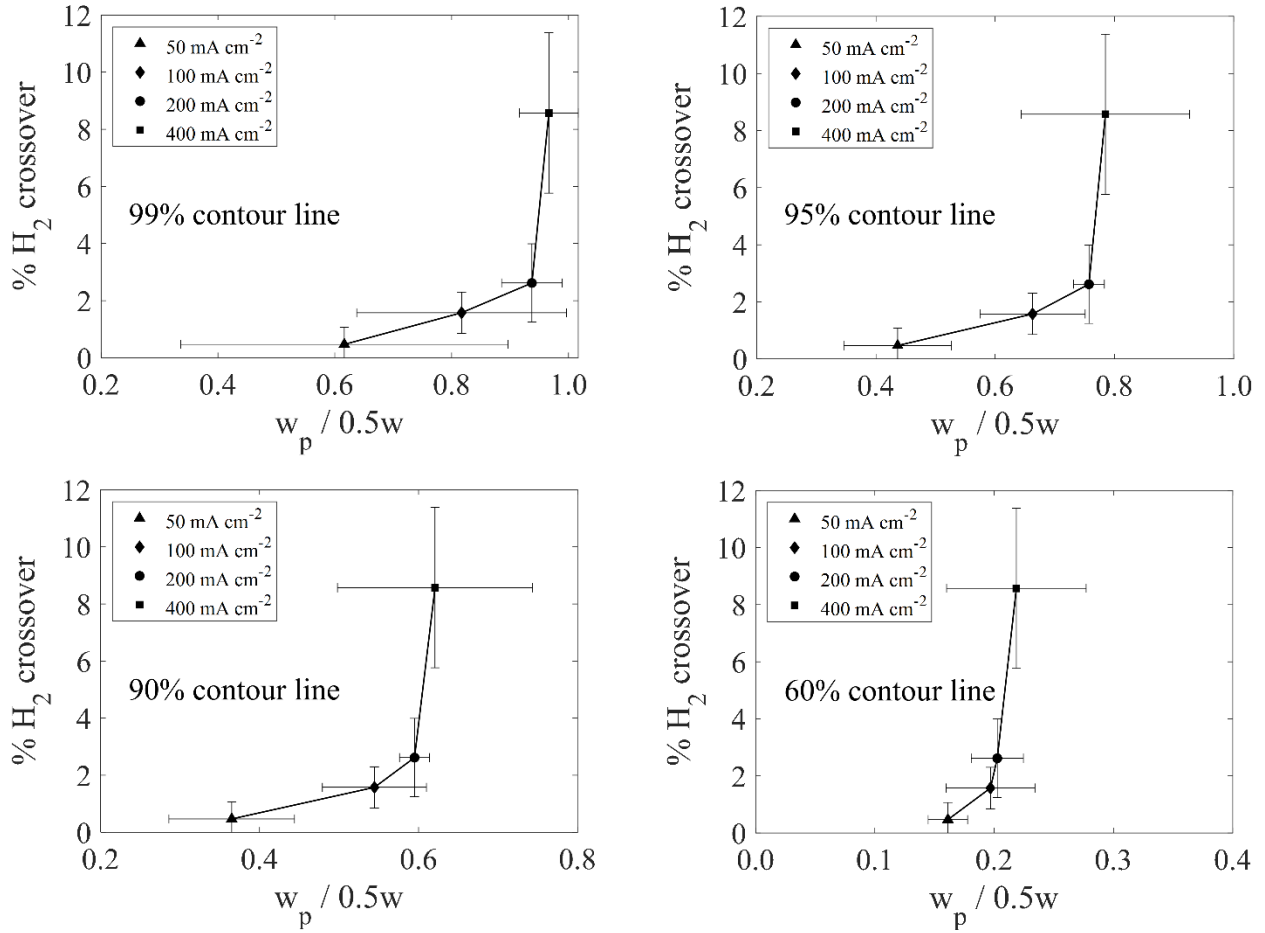


Figure S17: H₂ crossover as a function of normalized H₂ bubble plume width at different current densities for electrolysis at a constant *Re* of 131 when using different percentage contour line values ($X = 99\%$, 95% , 90% , 60%) as the normalized bubble plume widths. Channel width is 4 mm.

S18. H₂ plume width as a function of $Da^{0.47}$ in the laminar flow regime

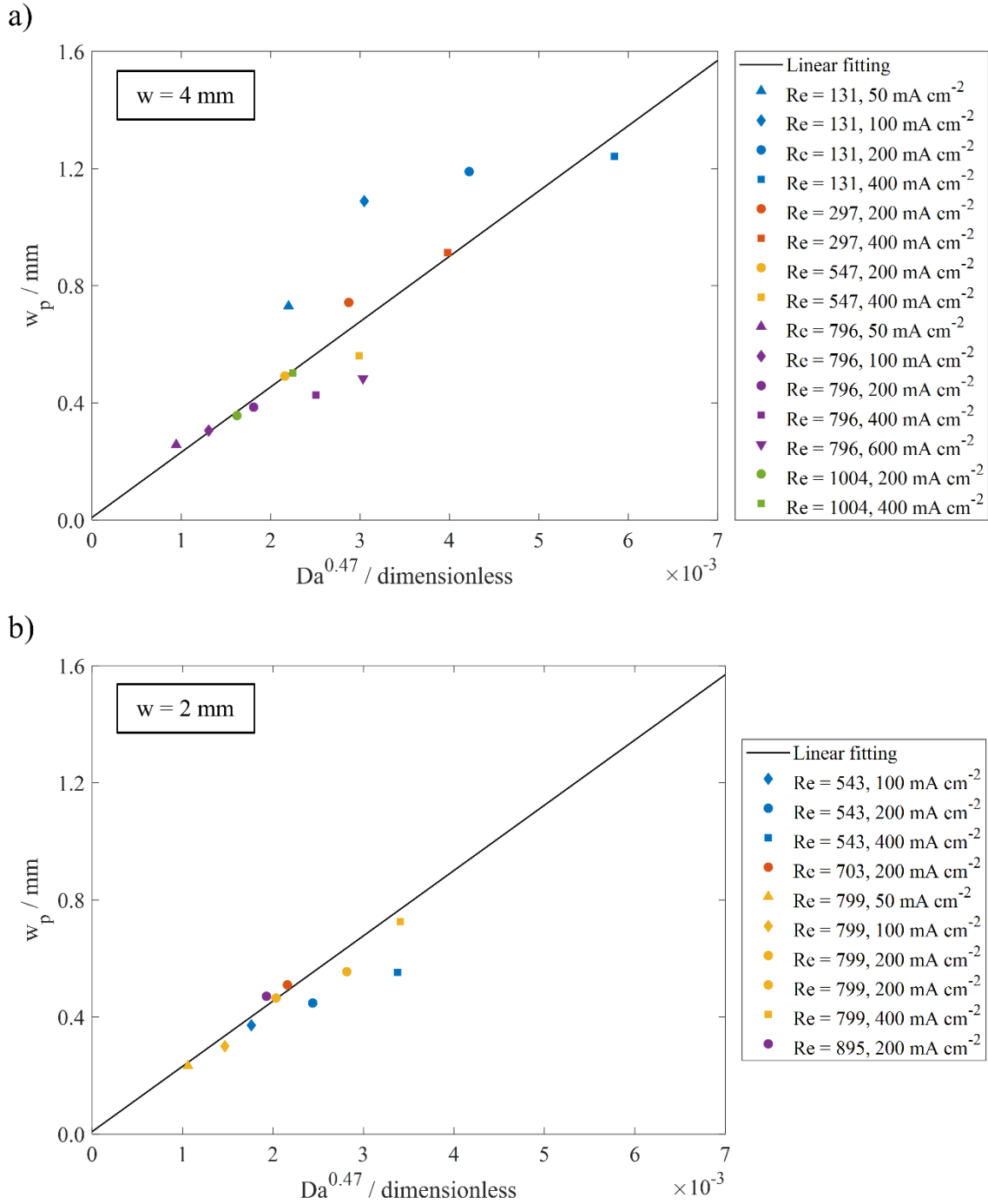


Figure S18: a) H₂ bubble plume width as a function of $Da^{0.47}$ for $w = 4$ mm at different current densities in the laminar flow regime with a linear fitting. b) w_p as a function of $Da^{0.47}$ for $w = 2$ mm at different current densities in the laminar flow regime with a linear fitting.

S19. Solution resistance as a function of channel width for different electrode lengths

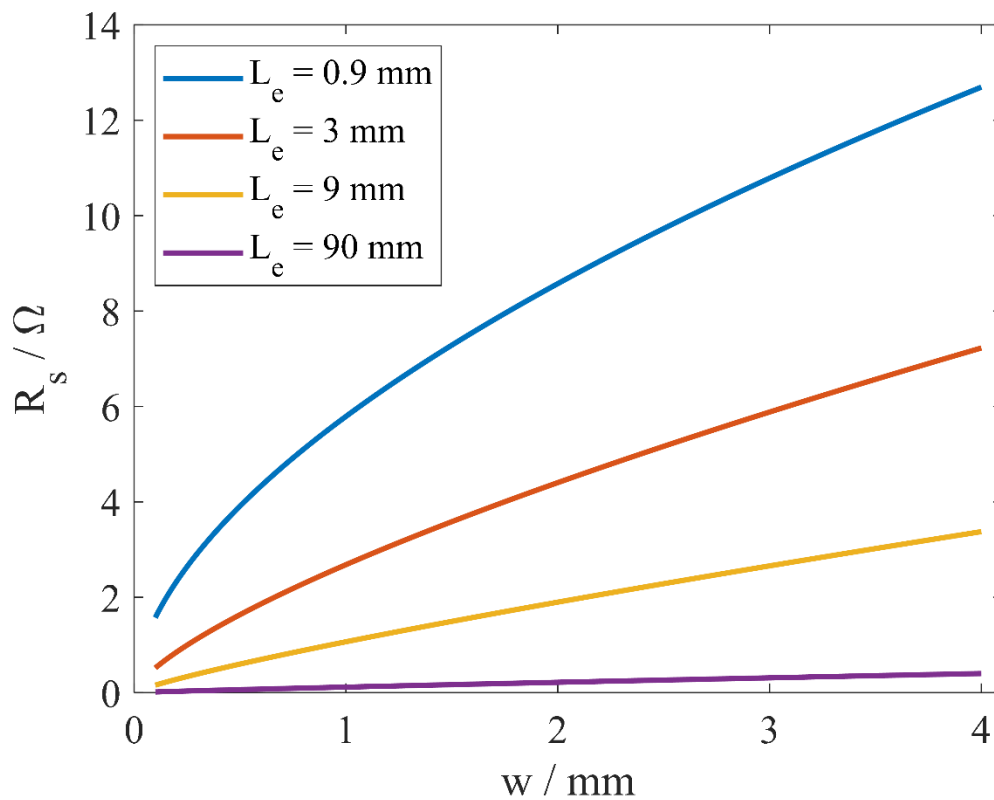


Figure S19: Simulated solution resistance as a function of channel width for different electrode lengths at a constant electrode height of $H = 3.34 \text{ mm}$ for an electrolyte of $0.5 \text{ M H}_2\text{SO}_4$ with a conductivity of 0.226 S cm^{-1} using COMSOL.

S20. Bubble-induced ohmic drop

The highest average void fraction for the imaging analysis region as shown in the purple box (Figure 3a) is 0.0145 for electrolysis at $Re = 131$ and $i = 400 \text{ mA cm}^{-2}$. The effectivity solution conductivity (κ) can be calculated using Bruggeman correlation³:

$$\kappa = \kappa_0(1 - \epsilon)^{3/2}$$

where κ_0 is the conductivity of the pure electrolyte, and ϵ is the void fraction.

$\kappa_0 = 0.226 \text{ S cm}^{-1}$, conductivity of 0.5 M H_2SO_4

For $\epsilon = 0.0145$, the calculated κ is 0.221 S cm^{-1} . Based on COMSOL simulation, ohmic resistance increases from $3.37 \text{ } \Omega$ to $3.44 \text{ } \Omega$ for $w = 4 \text{ mm}$, $h = 5 \text{ mm}$, $L_e = 9 \text{ mm}$ and $H = 3.34 \text{ mm}$ at $Re = 131$ and $i = 400 \text{ mA cm}^{-2}$. The ratio of additional ohmic drop due to bubbles to η_{Ω} in the bubble-free solution is calculated to be 0.021.

Void fraction is lower in between electrodes and higher flow rate gives rise to lower void fraction. In addition, less O_2 bubbles are generated compared with hydrogen, which leads to an even lower void fraction, hence, lower additional ohmic drop due to bubbles. The additional ohmic drop due to bubbles can be neglected.

S21. Current density-voltage curves from experimental measurement and 1D model

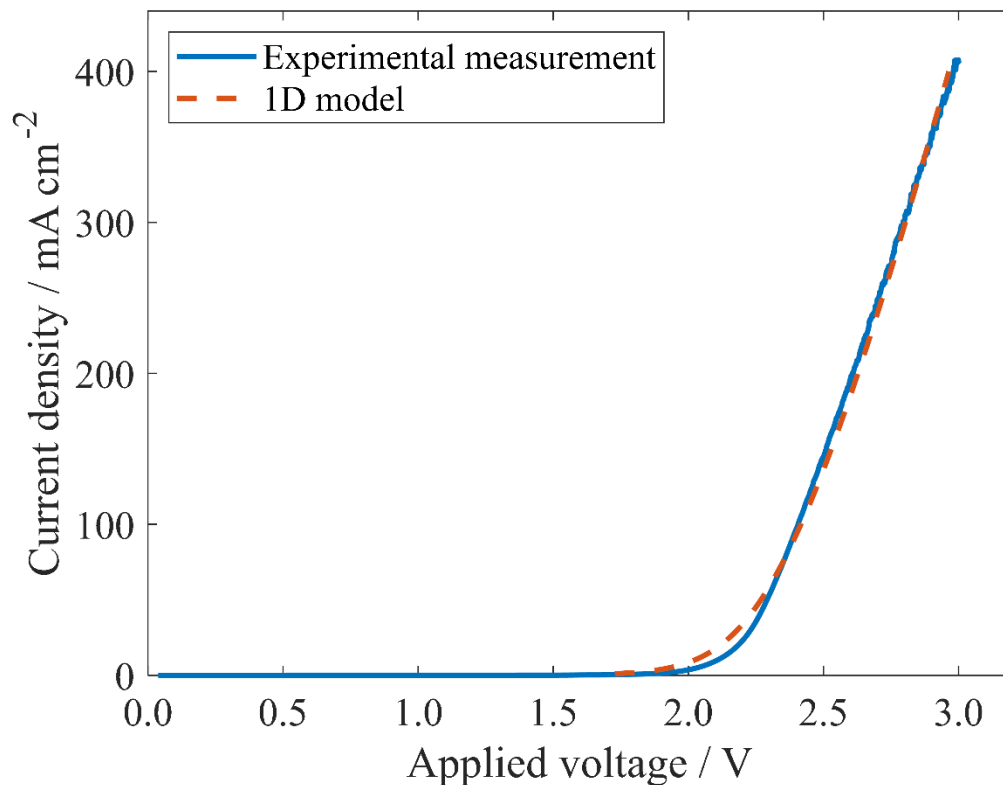


Figure S21: 2-electrode current density-voltage curves of water electrolysis with 0.5 M H₂SO₄ containing surfactant for an electrolyzer with 4 mm channel width at $Re = 547$. The blue solid curve is measured experimentally at 10 mV s^{-1} . The red dashed curve is generated using the 1D model presented in the paper using solution resistance measured by EIS during electrolysis and kinetic parameters obtained from literature for Pt HER electrocatalyst⁴ and fitted for Pt OER electrocatalyst.

S22. “Big bubble” departure event

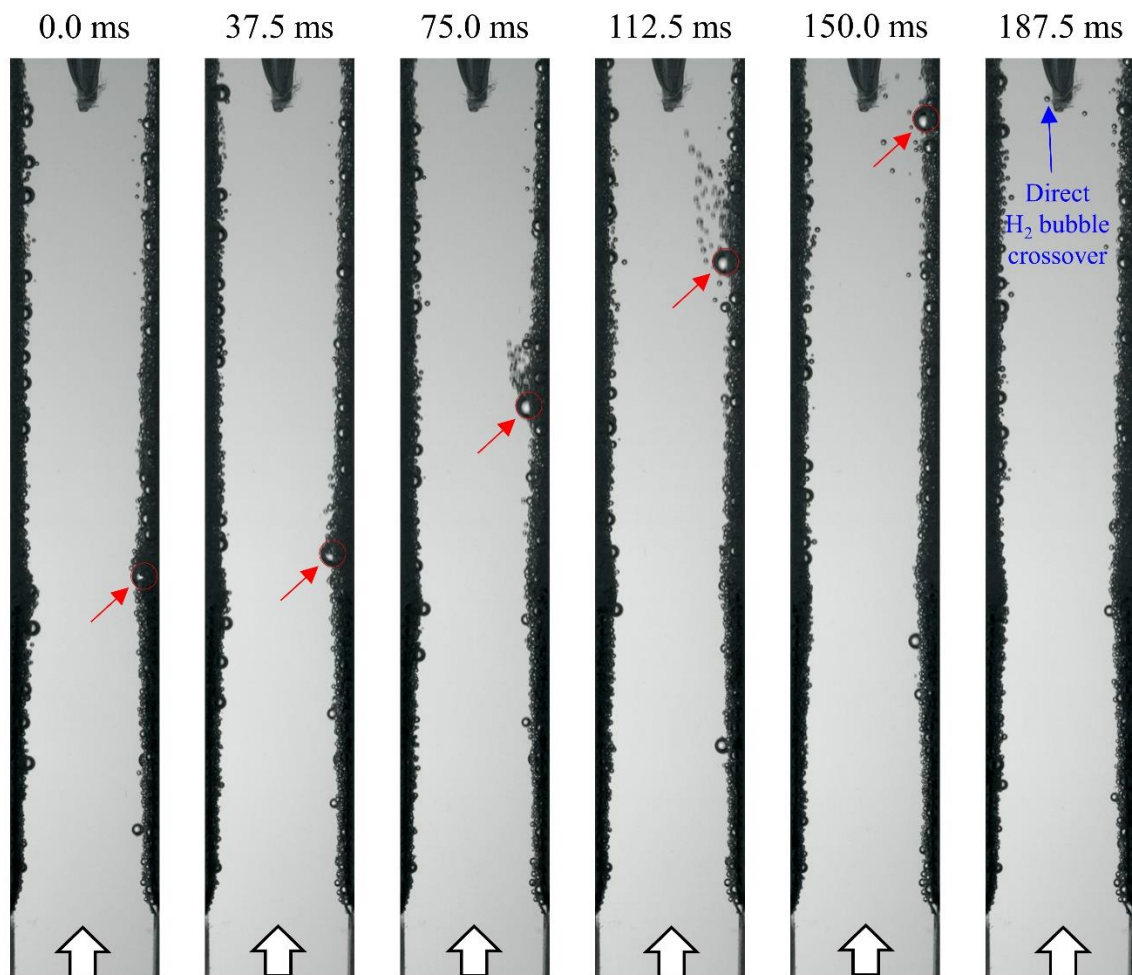


Figure S22: Representative still frame images from HSVs captured after 20 min of electrolysis showing a “big bubble” departure event, operated at 400 mA cm^{-2} and $Re = 547$ in surfactant-containing $0.5 \text{ M H}_2\text{SO}_4$. The “big bubble” is overlaid by a red circle to indicate its location at different time before it’s been separated by the divider. The electrolyzer channel width is $w = 4 \text{ mm}$, and the electrolyte flows from bottom to top in the image as indicated by the white arrows at the bottom of each image. The detachment of this “big bubble” leads to a direct crossover of a small bubble by promoting flow disturbance. This video has been uploaded as SI as well.

Video

Video is recorded at 1000 fps and plays at 30 fps.

Video S1: water electrolysis showing a “big bubble” departure event, operated at 400 mA cm^{-2} and $Re = 547$ in surfactant-containing $0.5 \text{ M H}_2\text{SO}_4$.

References

- 1 M. T. Janicke, H. Kestenbaum, U. Hagendorf, F. Schüth, M. Fichtner and K. Schubert, *J. Catal.*, 2000, **191**, 282–293.
- 2 N. de Nevers, *Fluid mechanics for chemical engineers*, McGraw-Hill, Third Edit., 1999.
- 3 M. Philippe, H. Jérôme, B. Sebastien and P. Gérard, *Electrochim. Acta*, 2005, **51**, 1140–1156.
- 4 H. Kita, S. Ye and Y. Gao, *J. Electroanal. Chem.*, 1992, **334**, 351–357.